AD-A105 639 DEFENCE RESEARCH ESTABLISHMENT VALCARTIER (QUEBEC) F/G 20/5
ANGLE OF ARRIVAL AND IRRADIANCE STATISTICS OF LASER BEAMS IN TU--ETC(U)
JUL 81 L BISSONNETTE, R COTE

UNCLASSIFIED DREV-R-4213/81 NL

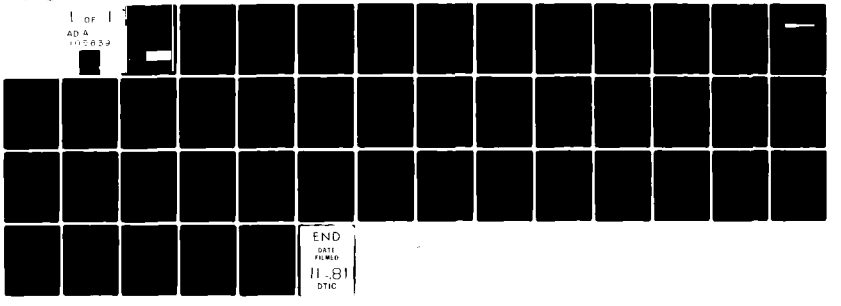

UNCLASSIFIED
UNLIMITED DISTRIBUTION

CRDV RAPPORT 4213/81
DOSSIER: 3633B-007
JUILLET 1981

DREV REPORT 4213/81
FILE: 3633B-007
JULY 1981

LEVEL 3

(3)

AD A105639

ANGLE OF ARRIVAL AND IRRADIANCE STATISTICS OF LASER BEAMS IN TURBULENCE

L. Bissonnette

R. Côté

Centre de Recherches pour la Défense
Defence Research Establishment
Valcartier, Québec

BUREAU - RECHERCHE ET DEVELOPPEMENT
MINISTÈRE DE LA DEFENSE NATIONALE
CANADA

RESEARCH AND DEVELOPMENT BRANCH
DEPARTMENT OF NATIONAL DEFENCE
CANADA

NON CLASSIFIE
DIFFUSION ILLIMITEE

CRDV R-4213/81
DOSSIER: 3633B-007

UNCLASSIFIED

(14) DREV-R-4213/81
FILE: 3633B-007

(12) 45

(6) ANGLE OF ARRIVAL AND IRRADIANCE
STATISTICS OF LASER BEAMS
IN TURBULENCE

by

(10) L./Bissonnette ~~and~~ R./Côté

CENTRE DE RECHERCHES POUR LA DEFENSE
DEFENSE RESEARCH ESTABLISHMENT
VALCARTIER
Tel: (418) 844-4271

(11) Jul 82

Québec, Canada

July/juillet 1981

NON CLASSIFIE

7 1945

RESUME

La mesure de l'angle d'arrivée en un point à l'intérieur d'un faisceau laser se propageant dans la turbulence est obtenue par la démodulation en fréquence du signal hétérodyne résultant de l'interférence d'un faisceau sonde avec un faisceau de référence. On utilise ensuite ces données pour démontrer que l'angle d'arrivée et l'intensité lumineuse sont faiblement correlés et que l'angle d'arrivée obéit à une distribution de probabilité normale. Ceci constitue une vérification directe de deux hypothèses fondamentales du modèle de propagation dans la turbulence mis au point au Centre de recherches pour la défense, Valcartier (CRDV). (NC)

ABSTRACT

Measurement of the local angle of arrival in a laser beam traveling in turbulence is achieved by frequency demodulating the heterodyne signal derived from the interference of a probe and a reference beam. The resulting data are then used to demonstrate that the statistical correlation between the angle of arrival and the irradiance is weak and that the random angle of arrival is normally distributed. These results constitute a direct confirmation of two fundamental assumptions of the theoretical model of propagation in turbulence previously developed at the Defence Research Establishment Valcartier (DREV). (U)

TABLE OF CONTENTS

RESUME/ABSTRACT i

1.0 INTRODUCTION 1

2.0 EXPERIMENTAL APPROACH 2

2.1 Experimental Apparatus 3
2.2 Heterodyne Detection 5
2.3 Angle of Arrival 10
2.4 Problem of Vibrations 15

3.0 RESULTS 21

3.1 Variance of the Angle of Arrival 21
3.2 Cross-Correlation of the Angle of Arrival with the Irradiance 26
3.3 Probability Distribution of the Angle of Arrival 29

4.0 DISCUSSION AND CONCLUSION 36

5.0 ACKNOWLEDGMENTS 37

6.0 REFERENCES 38

TABLES I AND II

FIGURES 1 - 10

1.0 INTRODUCTION

The phenomenon of turbulence has an important impact on optical and infrared laser applications in the atmosphere. It affects both high and low power beams and is generally more detrimental under clear, sunny conditions. The main resulting optical effects on laser beams are scintillation and beam spreading. Scintillation is a random modulation of the received irradiance. The amplitude of the modulation rapidly grows to a rms level of, the order of or even greater than, the average irradiance and the structure of the fluctuations is characterized by short and intense irradiance peaks, typically greater than 5 to 10 times the average irradiance. These modulations can obviously cause problems in communication coding or lower the breakdown thresholds at high power densities. Beam spreading is an average phenomenon whereby the many turbulent eddies along the propagation path act as scatterers that laterally diffuse the beam radiation. Although the average scattering angle remains relatively small, there results an important reduction in the beam power density at propagation distances of a few kilometers. Turbulence can indeed transform into a net loss the gain normally predicted by focusing the beam on the receiver.

We have developed at DREV a mathematical model that predicts the average irradiance and the irradiance variance profiles of laser beams propagating in turbulence (Refs.1-3). The model can also simulate the important practical situation where adaptive corrections are applied to the transmitted beam (Refs.4-5). The principal advantages of our approach over existing theories are that it is uniformly applicable at arbitrary scintillation levels, that the solutions are easily calculated numerically, and that extension to media with a varying and/or a non-linear average refractive index (e.g. thermal blooming in the presence of turbulence) is possible. The predictions are well corroborated by data measured in the atmosphere and in laboratory-simulated turbulence

(Refs.1-3). However, one basic assumption, although proven consistent, has not yet been verified directly. This assumption states that the instantaneous irradiance and the phase-front angle (or the angle of arrival of the optical rays) are only weakly correlated. In this report, we describe an experiment designed to measure simultaneously the local random irradiance and phase of a laser beam traveling in turbulence from where the hypothesis of weak correlation can be tested. The data obtained are also used to verify directly a second but less fundamental hypothesis which assumed normal statistics to relate the third- and fourth-order statistical moments of the angle of arrival to its second-order moments.

Section 2.0 reviews the experimental approach and Section 3.0 discusses the principal results.

This work was performed at DREV between January and December, 1980 under PCN 33B07, Atmospheric Propagation of Laser Beams.

2.0 EXPERIMENTAL APPROACH

The principal measurements presented in this report were obtained by a heterodyne detection method. This section describes the experimental apparatus and briefly reviews the theoretical equations pertinent to the present application. Also, this section discusses how and under what conditions the heterodyne signals are analyzed to obtain the turbulent variations of the angle of arrival.

2.1 Experimental apparatus

The objective of this work is to measure simultaneously the random fluctuations of the irradiance and the angle of arrival of a laser beam propagating in turbulence. The irradiance is obtained by ordinary incoherent detection but the angle of arrival to be determined necessitates a coherent heterodyne detection method. The latter consists in mixing on a detector the probe beam that propagates in the turbulence with a reference beam that travels outside of the turbulence in a homogenous medium. This constitutes an interferometer which allows the measurements of the relative phase between the two beams. Since the reference beam has constant parameters, the method yields the state of the instantaneous random phase of the beam in turbulence from which the angle of arrival is derived.

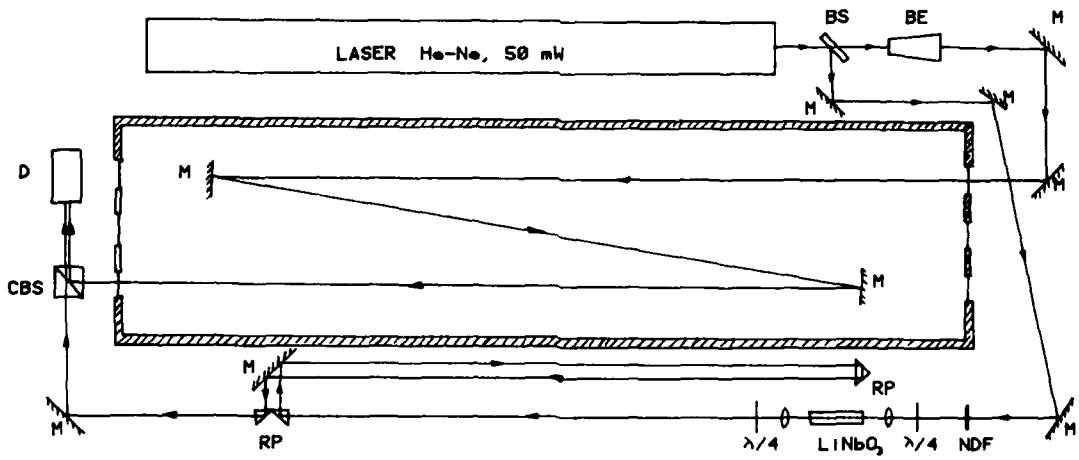

FIGURE 1 - Schematic diagram of the experimental apparatus. BS: beam splitter; BE: beam expander; M: front-surface mirror; NDF: neutral-density filter; λ/4: quarter-wave retardation plate; RP: right-angle prism; CBS: cube beam splitter; D: light detector.

The experimental apparatus is illustrated in Fig. 1. Both the probe and the reference beams are extracted from the same 50-mW He-Ne laser source. The reference beam is reflected from the front surface of a glass window positioned immediately at the exit of the laser; it has a 2-mm diameter and contains about 4% of the total power. The reflection from the back surface is blocked up. The transmitted part is expanded to a 25-mm diameter and constitutes the probe beam which is deflected by mirrors into the turbulent medium.

The turbulent medium is a scaled simulation of the atmosphere according to a technique described in Refs.6-7. In short, the refractive-index fluctuations are produced by creating an unstable vertical temperature gradient in a tank filled with water. This is simply done by heating the water at the bottom of the tank and cooling it at the top. The tank is 1.5 m long, 0.6 m deep, and 0.4 m wide. The characteristic Kolmogorov inertial subrange is reasonably well verified and the index structure constant C_n is typically 10^{-4} $m^{-1/3}$. The propagation axis is along the length of the tank and the distance can be increased by folding the beam as many times as required.

The measurement method for the angle of arrival is based on the frequency demodulation of the heterodyne signal obtained by mixing the probe and the reference beams. But, this approach is possible only if the modulation caused by the fluctuating angle of arrival is carried by a higher frequency signal, which is done here by shifting the optical frequencies of the probe and the reference beams with respect to one another. Considering all the operating conditions, we find that a convenient shift should be of a few kilohertz. Reference 6 gives a review of several techniques of optical frequency shifting available in this range, but the one best suited to our needs is the use of an electro-optic crystal. As applied in the present experiment and illustrated in Fig. 1, the technique consists in letting the reference beam

propagate through a 30-mm-long, 1 x 1 mm^2 crystal of $LiNbO_3$ excited by a transverse electric field rotating at a frequency $\Omega/2\pi$. The latter is simply produced by applying two sinusoidal voltages of equal amplitude (nominally 200 V) and in quadrature to the lateral faces of the crystal. The principle of operation, outlined in Ref. 6, is that the rotating electric field inside the crystal has the property of accelerating (or decelerating) the incident circularly polarized field of the laser light beam, thus creating an upshift Ω (or downshift) of the angular optical frequency of the outgoing light. The method is equivalent to a rotating half-wave plate and the efficiency quoted in Ref. 6 is 55%, which is well corroborated by our measurements. Two $\lambda/4$ - phase retardation plates are used to transform the linear polarization of the reference beam into circular polarization and vice versa. The first lens focuses the beam inside the crystal for better efficiency and the second one recollimates it. Following the frequency shifter, a set of right-angle prisms is arranged to adjust the propagation path of the reference beam to that of the probe beam. This is necessary since the longitudinal coherence length of the laser is only a few tens of centimeters. Finally, the two beams are brought together or mixed by a 50-mm cube beamsplitter as shown in Fig. 1; the interfering beams are then detected by a silicon phototransistor mounted behind a 0.5-mm-diameter aperture.

2.2 Heterodyne Detection

The reference and the probe beams are linearly polarized in the same direction and, as is customary and justified (Ref. 7, p. 93, eqs. 6.1 and 6.2) in the treatment of atmospheric turbulence, it is assumed that polarization is not affected by propagation. A scalar representation is therefore possible and the electric field E in the respective beams is denoted as follows:

$$E_p = A_p \exp[-i\omega_p t + ik\, n_{op}\, z_p + ik\, n_{op}\, \phi_p], \qquad [1]$$

$$E_r = A_r \exp[-i\omega_r t + ikn_{or}z_r + ik_r n_{or}\phi_r] \ , \qquad [2]$$

where A is the amplitude, ω is the optical angular frequency, k is the free-space optical wave number, c is the speed of light in free space, n_o is the unperturbed index of refraction of the medium, z is the geometrical distance of propagation, ϕ is the phase shift, i.e. the difference between the optical and the geometrical thicknesses of the propagation medium, and $i = \sqrt{-1}$. The subscripts r and p refer to the reference and the probe beams respectively. The two beams are mixed and aligned parallel to each other on a photodetector which thus gives a current

$$j \propto (E_p + E_r)(E_p + E_r)^* \ , \qquad [3]$$

where the superscript * denotes a complex conjugate. Substituting eqs. 1-2 for E_p and E_r in eq. 3 and assuming that $\Omega = \omega_r - \omega_p$ is much smaller than either ω_r or ω_p, we find

$$j \propto A_r^2 + A_p^2 + 2A_r A_p \cos[\Omega t + k(n_{op}\phi_p - n_{or}\phi_r) + k(n_{op}z_p - n_{or}z_r)]. \qquad [4]$$

For detection at a given fixed point, the parameters A_r, ϕ_r, z_r, z_p, n_{or}, n_{op}, Ω and k are constant. Hence, eq. 4 can be more conveniently rewritten

$$j \propto A_r^2 + A_p^2 + 2A_r A_p \cos[\Omega t + kn_{op}\phi_p + cst] \ , \qquad [5]$$

where cst is a constant that regroups the remaining invariant parameters. The quantities of interest to the present study are A_p^2 and ϕ_p, respectively the irradiance and the phase of the probe beam that has traveled through the turbulence.

The requirement of the following analysis is to derive both quantities A_p^2 and ϕ_p from the single heterodyne signal given by eq. 5. A simple examination of eq. 5 shows that by choosing the frequency shift $\Omega/2\pi$ much greater than the highest frequencies of the turbulent irradiance A_p^2, it is possible to separate electronically the first two terms from the last one. Indeed, if the cutoff frequencies are properly set, a low-pass filter will yield a signal

$$e_{lp} \propto A_r^2 + A_p^2 , \qquad [6]$$

and a high-pass filter, a signal

$$e_{hp} \propto A_r A_p \cos[\Omega t + kn_{op}\phi_p + cst]. \qquad [7]$$

Since A_r is constant, it is easy to subtract its contribution from eq. 6 and we thus obtain a signal proportional to the fluctuating irradiance A_p^2 of the probe beam at the position of the detector.

The electronic signal given by eq. 7 is a signal at frequency $\Omega/2\pi$ modulated in amplitude by A_p and in frequency by ϕ_p. This is well illustrated in Fig. 2, where two time records of the high-pass filtered signal are reproduced: a first one at a slower sweep rate to show the

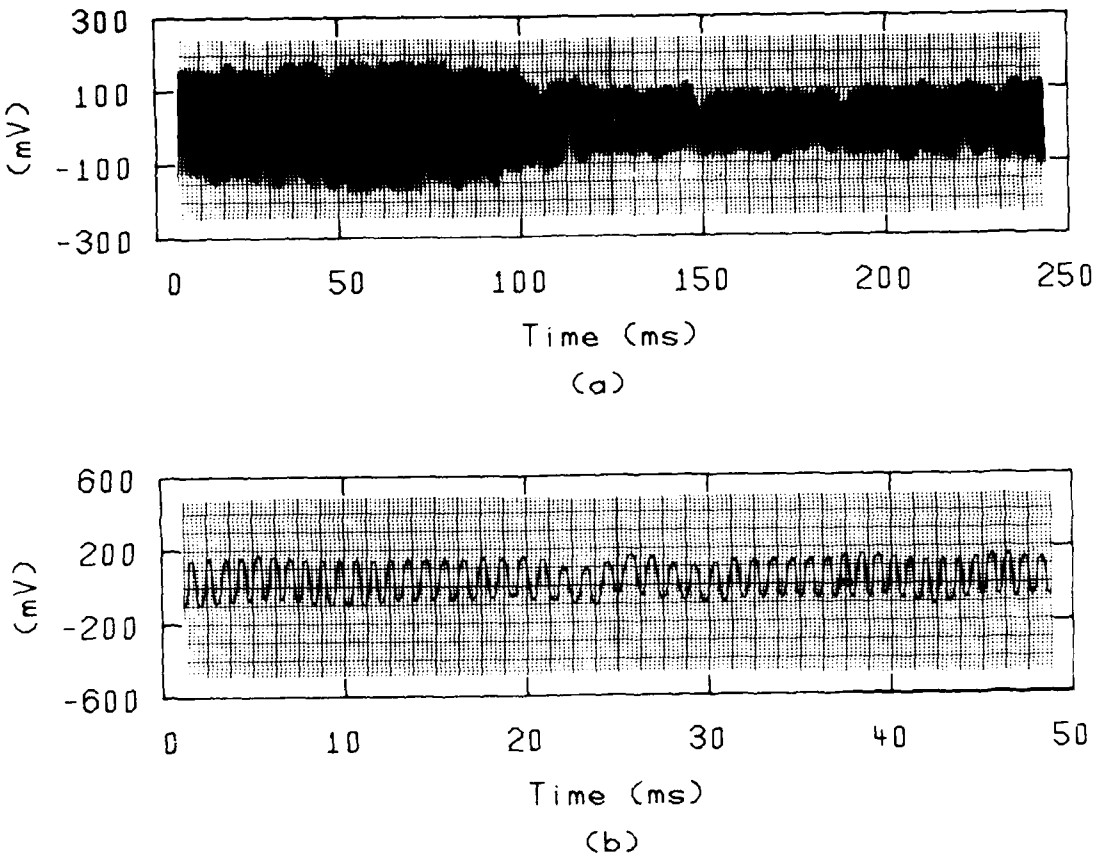

FIGURE 2 - Example of a detected heterodyne signal modulated in amplitude and frequency by the turbulence; propagation distance $z = 1.62$ m. Trace (a): slower sweep rate to exemplify the amplitude modulations. Trace (b): faster sweep rate to exemplify the frequency modulations.

amplitude modulations and a second, at a faster sweep rate to show the frequency modulations. Since the frequency domain of A_p is much smaller than $\Omega/2\pi$, the characteristic amplitude-modulation periods extend over many oscillations at frequency $\Omega/2\pi$. Therefore, it is possible, in principle, to frequency demodulate the signal of eq. 7 independently of the amplitude modulations and thus obtain the time derivative of the phase ϕ_p. This is the approach chosen in the present experiment.

The apparatus used to perform the frequency demodulation is a Doppler Signal Processor designed for laser anemometry and built by DISA ELEKTRONIK A/S. Omitting the details of the electronics which can be found in Ref. 8, this apparatus delivers an output voltage proportional to the instantaneous frequency of the input signal it tracks, i.e. proportional to the time derivative of the cosine argument of eq. 7. The output voltage of the Doppler Signal Processor is thus

$$e_{dp} = K[\Omega + kn_{op} \frac{d\phi_p}{dt}], \qquad [8]$$

where K is the calibration constant. This output voltage e_{dp} will, hereafter, often be referred to as the frequency-demodulated heterodyne signal. The frequency $\Omega/2\pi$ is adjustable but, for most results reported here, it was set at 4.5 kHz. The Signal Processor was operated in the frequency range of 2.25 to 15 kHz which gives an upper tracking frequency limit for $d\phi_p/dt$ of about 100 Hz (Ref. 8). This limit is quite sufficient for the type of turbulence studied here as the results will show. Finally, the tracker sensitivity in this range is K =0.100 ±0.002 mV/rad/s determined from the slope of an experimental voltage-frequency calibration curve.

2.3 Angle of Arrival

The quantity derived from the analysis of the tracker output is $d\phi_p/dt$. However, our purpose is to measure the instantaneous angle of arrival. Following our propagation model developed in Refs. 1-3, the angle of arrival $\underset{\sim}{\gamma}$ at point $(z, \underset{\sim}{r})$ is defined as the vector angle subtended by the geometrical ray which passes through the point $(z, \underset{\sim}{r})$; z is the propagation distance and $\underset{\sim}{r}$, the position vector in the plane perpendicular to the propagation axis. From Refs. 1-3, we thus have in the notation of this report

$$\underset{\sim}{\gamma}(z, \underset{\sim}{r}) \simeq \underset{\sim}{\nabla}\phi_p (z, \underset{\sim}{r}), \qquad [9]$$

where $\underset{\sim}{\nabla}$ is the gradient operator with respect to the coordinates of $\underset{\sim}{r}$. Hence, we need to relate $d\phi_p/dt$ to $\underset{\sim}{\nabla}\phi_p$. *The sign* $\simeq$ is used in eq. 9 instead of = because the definition of the phase ϕ_p differs slightly from that of Refs. 1-3. On the one hand, the phase ϕ used in Refs. 1-3 satisfies the eikonal equation of geometrical optics, i.e.

$$\frac{\partial\phi}{\partial z} + \frac{1}{2}(\underset{\sim}{\nabla}\phi)^2 = (N-n_o) \quad , \qquad [10]$$

where N is the instantaneous index of refraction of the medium and where the paraxial approximation, valid for the propagation in atmospheric turbulence, has been made. On the other hand, the phase ϕ_p of eq. 1 is the sum of ϕ plus a contribution due to diffractional effects since the amplitude in eq. 1 is taken as real. However, diffraction contributes only slightly to the fluctuations of ϕ_p and from here on, we will set $\phi_p \simeq \phi$.

The turbulent angle of arrival $\underset{\sim}{\gamma} = \underset{\sim}{\nabla}\phi$ is generally small, typically smaller than 1 mrad, even in very strong scintillation. Hence, the nonlinear term in eq. 10 can be neglected with good accuracy and we derive

$$\frac{d\phi}{dt} = \int_0^z dz \left(\frac{\partial N}{\partial t} + W \frac{\partial N}{\partial z} + \underset{\sim}{U} \cdot \underset{\sim}{\nabla} N \right) \quad , \qquad [11]$$

where W and $\underset{\sim}{U}$ are respectively the fluid velocity components along and normal to the propagation axis. The first term on the right-hand side of eq. 11 is negligible since it represents the temporal index variations only, i.e. after the fluctuations due to spatial movements of the fluid have been left out. These temporal variations are generally much slower, so that $|\partial N/\partial t| << |\underset{\sim}{U} \cdot \underset{\sim}{\nabla} N|$. Similarly, the second term is also neglected since the rapid fluctuations of $\partial N/\partial z$ are averaged out by the integration over z, which is not the case for the transverse derivative $\underset{\sim}{\nabla} N$. Moreover, as will be seen in the following discussion, the velocity component W in the regions that contribute most to the integral is much smaller than $\underset{\sim}{U}$. Hence, eq. 11 is simplified to

$$\frac{d\phi}{dt} \simeq \int_0^z \underset{\sim}{U} \cdot \underset{\sim}{\nabla} n \, dz \quad . \qquad [12]$$

The unstable temperature convection that characterizes boundary layers with low velocity, as is the case in the atmosphere and in our turbulence simulator, has the structure of vertical jets or plumes. The warmer and more turbulent fluid rises in these jets while the cooler and less turbulent fluid sinks in more uniform and less localized currents. This phenomenon, briefly discussed in Refs. 9-10, helped

explain the observed intermittency of the temperature fluctuations recorded in our simulator. Three important properties of this structure of unstable convection are used to further simplify eq. 12. Firstly, the level of temperature or refractive-index turbulence is higher inside the jets. Although no systematic measurements of these differences have been carried out in our simulator, the results of Refs.9-10 indicate that a factor of 3-5 is probably correct. Secondly, the fluid velocity inside the jets is greater than the sinking velocity by a factor of 4 to 5 (Ref. 11, p. 147). Finally, the rising velocity is approximately constant over most of the jet cross section. Therefore, the contributions to the integral of eq. 12 come mainly from the optical-path segments that pass through these jets. Hence, if we assume that the jets have an average rising velocity $\overline{U}$, we can approximate eq. 12 as follows:

$$\frac{d\phi}{dt} \simeq \overline{U} \int_0^z \frac{\partial}{\partial y} N \, dz \ , \qquad [13]$$

where y is the vertical coordinate. In other words, the horizontal motion, including the component W, is less important and contributes little to $d\phi/dt$. Finally, from the definition of the angle of arrival $\underset{\sim}{\gamma} = \underset{\sim}{\nabla}\phi$ and the approximation of linearization, we obtain from eq. 10

$$\underset{\sim}{\gamma}(z, \underset{\sim}{r}) = \int_0^z \underset{\sim}{\nabla} N \, dz \ . \qquad [14]$$

Therefore, comparing eq. 13 to eq. 14, we find

$$\frac{d\phi}{dt} \simeq \bar{U}\, v_y \,, \qquad [15]$$

where v_y is the component of $\underset{\sim}{v}$ in the vertical direction.

Equation 15 relates the temporal derivative of the turbulent phase fluctuations, measured by demodulating the heterodyne signal, to the vertical component of the angle of arrival. This equation was derived through a series of approximations difficult to verify individually. However, the data analysis will show that eq. 15 is consistent and can indeed be used for the present purpose of calculating the statistical correlation between the irradiance and the angle of arrival, and the probability distribution of the latter.

2.4 Problem of Vibrations

In the expression for the heterodyne signal (eq. 5), we have collected in a single additive constant all the contributions related to the geometrical propagation paths z_p and z_r. This is justified in principle since the detection is made at a fixed point. In practice, however, there are oscillations in the relative path difference which can obscure the useful turbulent phase signal. From the expected magnitude of the turbulent phase fluctuations, we realize that oscillations in $(z_p - z_r)$ of amplitude as small as 1 μm are sufficient to do this. Such oscillations are difficult to eliminate completely.

To minimize this problem, all the components of the experimental setup, including the turbulence simulator, were mounted on a vibration-isolated table. The improvement over the nonisolated conditions is substantial but insufficient to consistently bring the noise level due

to the vibrations well below the signal level. Figure 3 shows an example of a measured spectral-density function of the frequency demodulated heterodyne signal. This density function was calculated with a HONEYWELL SAICOR-42A Correlation and Probability Analyzer interconnected with a HONEYWELL SAICOR-470 Fourier Transform Analyzer; the electronic signal was sampled at a rate of 500 Hz, and 2^{17} points were used for the computations. We observe in the spectrum of Fig. 3 an important peak centered at about 32 Hz. This contribution, which accounts for a large fraction of the total power, is caused by the vibrations. Extensive investigations indicate that the position of the peak is practically independent of the various noise sources in the laboratory, pointing to a phenomenon of resonance. However, this contribution cannot be removed by simple electronic filtering since it occurs well inside the expected frequency bandwidth of $d\phi/dt$, the signal of interest. Moreover, satisfactory elimination by mechanical isolation would require extreme care especially because of the large number of components involved. Therefore, a modified approach to the measurements was designed to minimize the effects of vibrations while satisfying the requirements of this study.

The vibration frequencies observed in the typical spectral-density function plotted in Fig. 3 are sufficiently low to suggest that the responsible optical components oscillate in their fundamental mode. This means that the components vibrate as a solid block and that higher-order rotation or torsion modes are unlikely. If this is correct, the vibrations should have the same effect irrespective of the measurement position across the beam. Therefore, if the heterodyne signals were recorded simultaneously at two points on the beam cross section and if the resulting frequency-demodulated signals were subtracted, the vibration contributions should cancel out. This is the technique we have selected and Fig. 4 illustrates how it is implemented. The reference beam is split into two parallel beams and both portions are mixed with

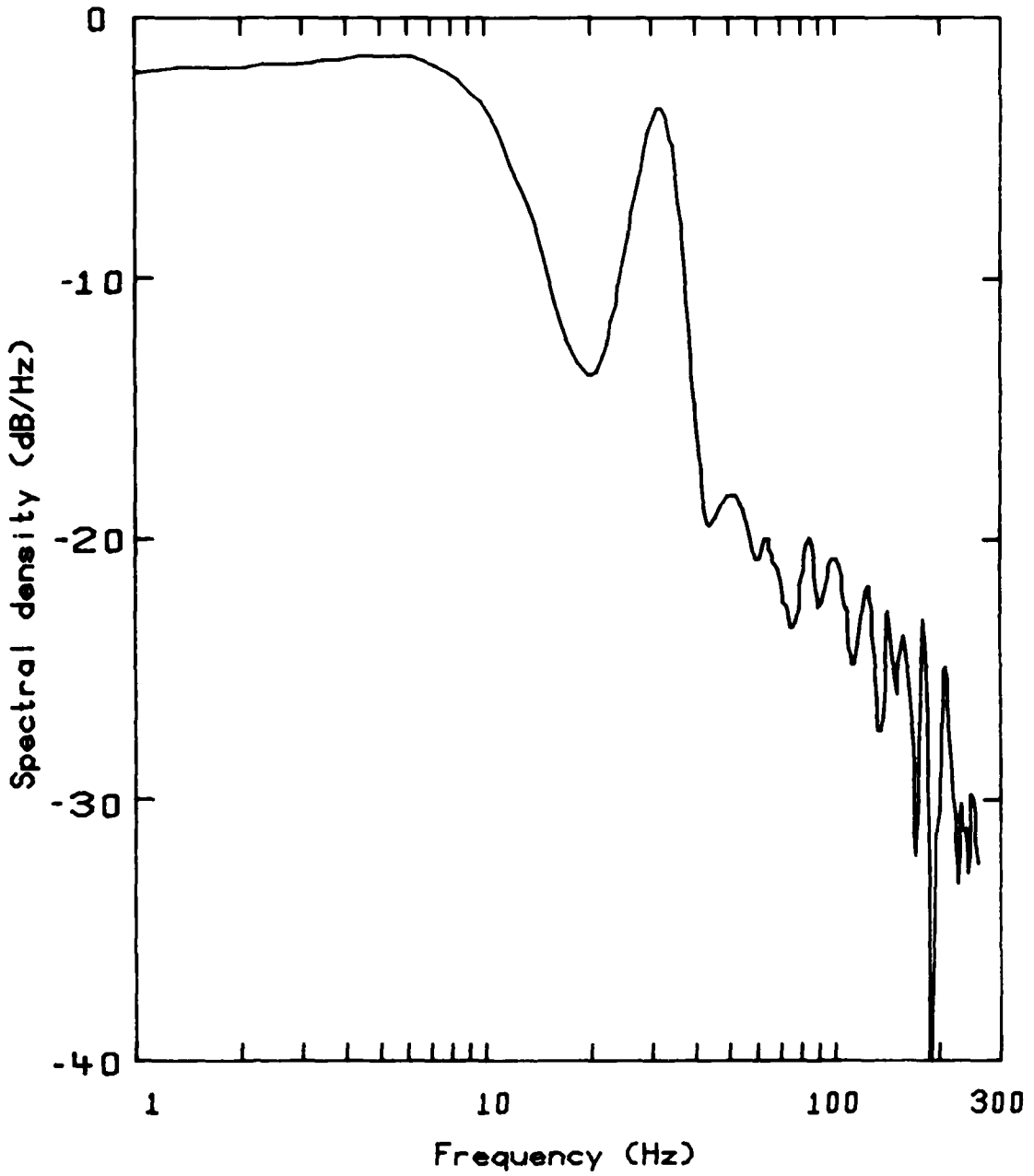

FIGURE 3 - Example of the measured spectral density of the frequency-demodulated heterodyne signal detected at one point. The peak centered at about 32 Hz is due to the effects of mechanical vibrations.

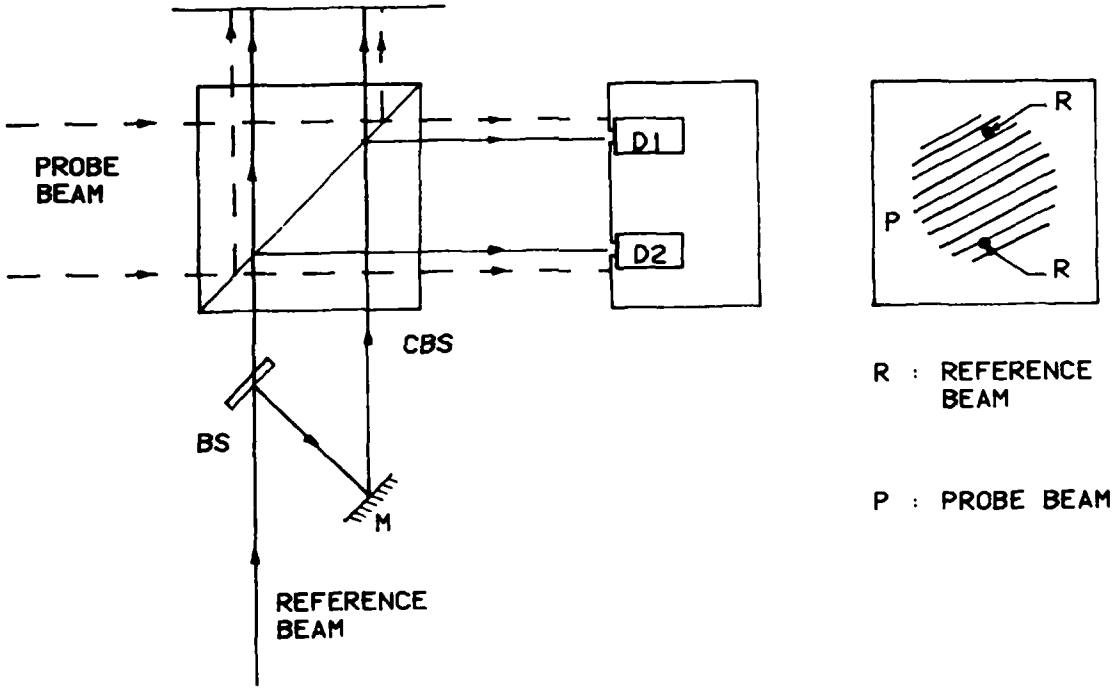

FIGURE 4 - Schematic diagram illustrating the technique for simultaneous heterodyne detection at two points in the probe-beam cross section. BS: beam splitter; CBS: cube beam splitter; D1, D2: light detectors.

the 25-mm-diameter probe beam. The interfering beams are then detected simultaneously. The measurement points are 15 mm apart, positioned at approximately equal distance from the beam axis.

Ideally, the technique would require two Doppler Signal Processors to demodulate simultaneously the two heterodyne signals. Since only one was available, the analysis was performed in two consecutive operations as shown in Fig. 5. In the first operation (Fig. 5a), one of the high-pass filtered heterodyne signals was recorded on one channel of a magnetic tape recorder while the second signal was demodulated and the output of the processor recorded on a second channel. Logarithmic amplifiers were used to reduce the turbulent amplitude modulations. Also recorded in this first operation were the low-pass filtered signals, i.e. the irradiance fluctuations at both points. In the second operation (Fig. 5b), the tape was played back and the recorded heterodyne signal was demodulated in its turn. The output was then subtracted from the previously recorded demodulated signal. The resulting voltage is thus proportional to the required function $(d\phi_1/dt - d\phi_2/dt)$ where the subscripts 1 and 2 refer to the two points of measurement.

Figure 6 shows the spectral density function of $(d\phi_1/dt - d\phi_2/dt)$ for the same time segment as for the corresponding spectral density of $d\phi_1/dt$ plotted in Fig. 3. The peak at 32 Hz has almost completely disappeared suggesting that the vibration contributions have cancelled out. To further illustrate how the technique works, we have also reproduced in Fig. 7 time recordings of $d\phi_1/dt$ and $(d\phi_1/dt - d\phi_2/dt)$ for nonturbulent conditions. In the latter case, $(d\phi_1/dt - d\phi_2/dt)$ should be zero everywhere. We find that the signal level has indeed dropped, by a factor of about 5 in rms values, and that the periodic oscillations have been eliminated by subtraction. Hence, the method eliminates efficiently the effects of mechanical vibrations and modifies only slightly the analysis of the data. The residual noise is attributed to

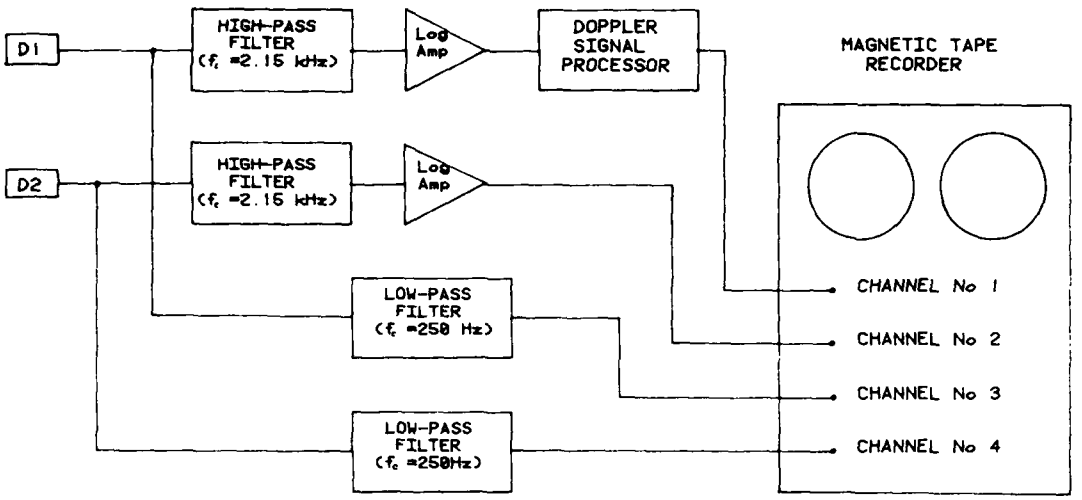

(a)

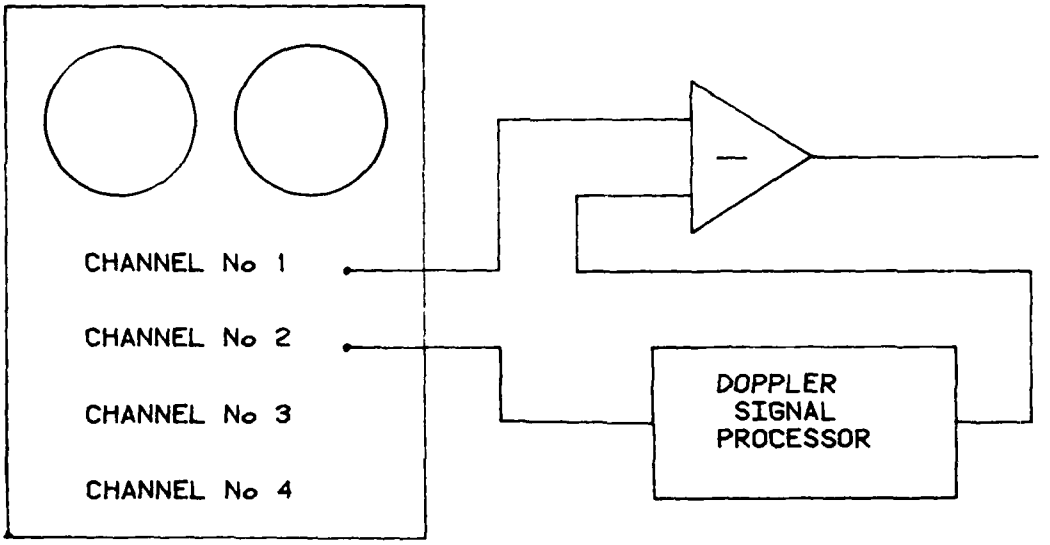

(b)

FIGURE 5 - Block diagram of the electronic processing of the heterodyne signals. (a) recording operation; (b) playback operation. D1, D2: light detectors.

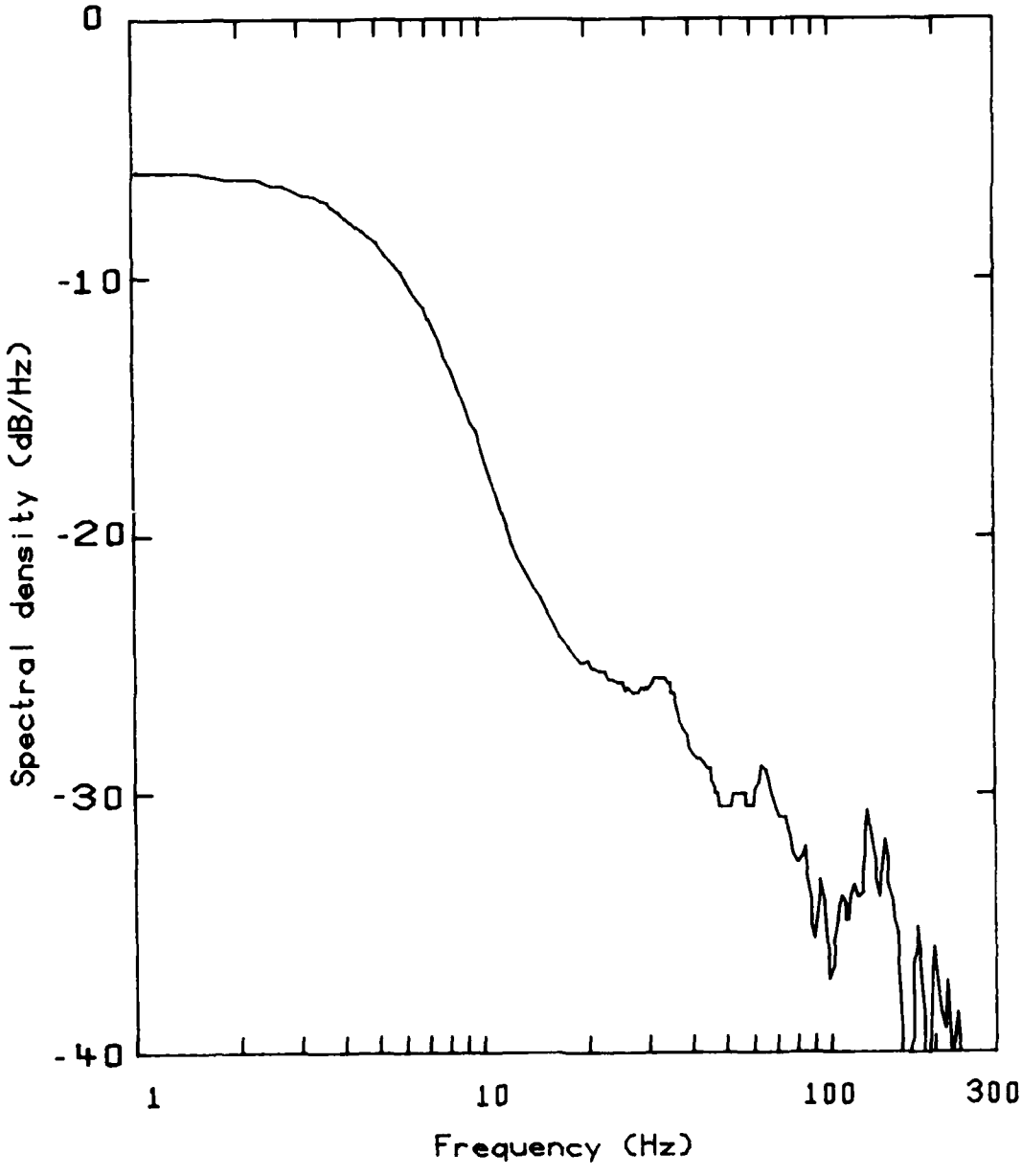

FIGURE 6 - Example of the measured spectral density of the difference between the frequency-demodulated heterodyne signals detected simultaneously at two points. The contributions due to the mechanical vibrations have cancelled out almost completely.

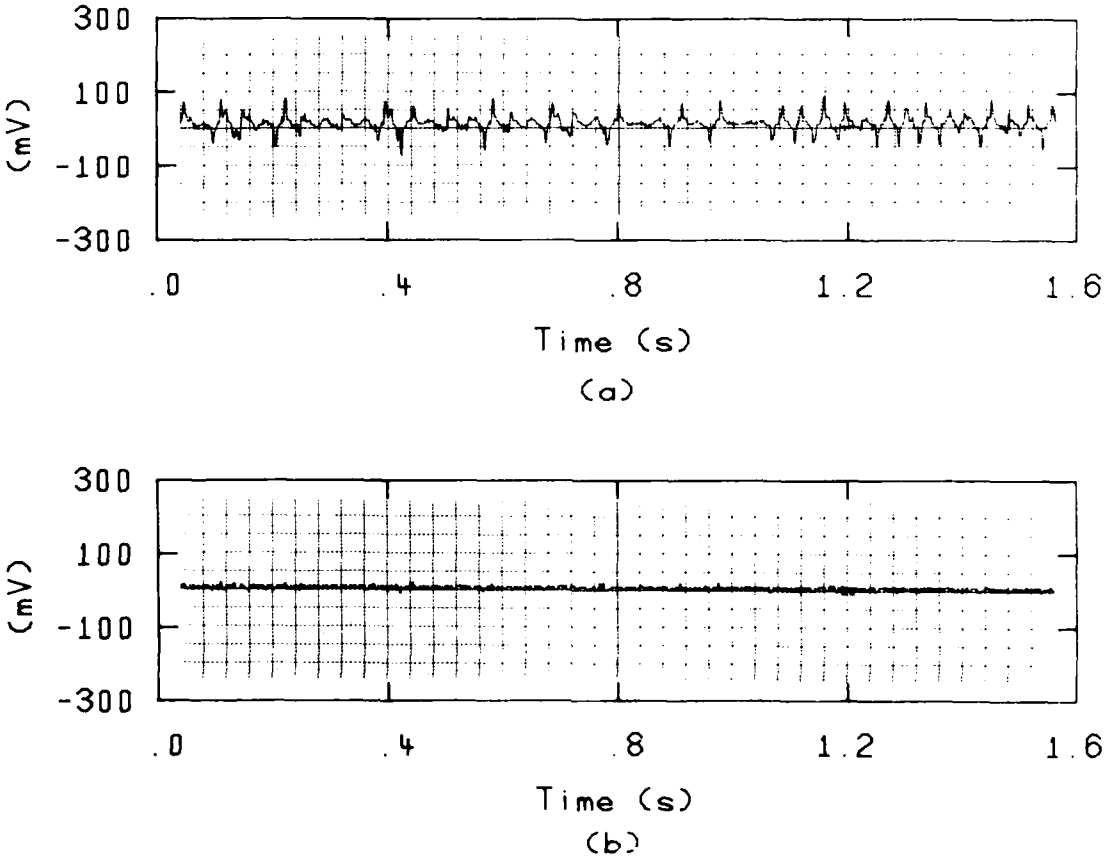

FIGURE 7 - Example of cancellation of the effects of mechanical vibrations. Trace (a): time recording of the frequency-demodulated heterodyne signal detected at one point. Trace (b): time recording of the difference between the frequency-demodulated heterodyne signals detected simultaneously at two points separated by 15 mm in the probe-beam cross section. The recordings were made under conditions of vanishing turbulence.

the electronic processing, in particular to the Doppler Signal Processor. The following sections will discuss how the useful signal and the processing noise are separated for each application.

3.0 RESULTS

3.1 Variance of the Angle of Arrival

From eqs. 8 and 15 and the assumption that the contributions due to the vibrations cancel out exactly, the difference between the output voltages of the Doppler Signal Processor for the two measurement points $\underset{\sim}{r}_1$ and $\underset{\sim}{r}_2$ is given by

$$e_1 - e_2 = Kkn_o\overline{U}\,[v_y(\underset{\sim}{r}_1) - v_y(\underset{\sim}{r}_2)]. \qquad [16]$$

The variance of $(e_1 - e_2)$ is therefore proportional to the structure function of the angle of arrival for a separation distance $\underset{\sim}{\Delta} = \underset{\sim}{r}_1 - \underset{\sim}{r}_2$ which was chosen along the horizontal axis, i.e. $\underset{\sim}{\Delta} = \Delta\underset{\sim}{i}$. From the theoretical results of Ref. 3 on the covariance of the angle of arrival, we then have

$$\langle(e_1-e_2)^2\rangle = K^2k^2n_o^2\,\overline{U}^2\,\langle(v_y(\underset{\sim}{r}_1) - v_y(\underset{\sim}{r}_2))^2\rangle$$

$$= 6.90\,\frac{K^2k^2n_o^2\overline{U}^2C_n^2z}{\ell_o^{1/3}}\left\{1 - [1+8.16\,\Delta^2/\ell_o^2]^{-1/6}\right\}, \qquad [17]$$

where the pointed brackets <...> denote ensemble averaging and where C_n is the refractive-index structure constant, ℓ_o is the inner scale of turbulence, and z is the propagation distance.

Equation 17 is a variant of eq. 15 which relates the measured time derivative of the turbulent phase to the angle of arrival. As discussed previously, eq. 15 is central to the present analysis but it is based on a series of approximations difficult to verify individually. However, eq. 17 now provides a means of determining its consistency. To do this, the variance of $(e_1 - e_2)$ was measured at several propagation distances leaving all the other parameters constant. Equation 17 shows that these data, when plotted against z, should fall on a straight line through the origin, which is reasonably well confirmed by Fig. 8.

The contributions due to the processing noise that are subtracted from the data of Fig. 8 were calculated by recording the heterodyne signal of one of the detectors along with the demodulated signal from the same detector. On playing back the tape and performing the same analysis as for $\langle(e_1 - e_2)^2\rangle$, we thus obtain the residual noise level. This procedure was repeated for all the data points of Fig. 8 and we found that the noise was constant to within ± 8%. All the variances were measured with the HONEYWELL SAICOR-42A Correlation and Probability Analyzer from 2^{17} samplings of the instantaneous electronic signals digitized at a rate of 500 Hz.

The processing noise has its origin in the strong turbulent amplitude fluctuations of the heterodyne signal characterized by intense peaks followed by periods of vanishing amplitude. If, during these periods, the signal drops below a preset threshold, the Doppler Signal Processor breaks its servo loop and holds its output until the signal reappears at a frequency within certain limits of the last measured

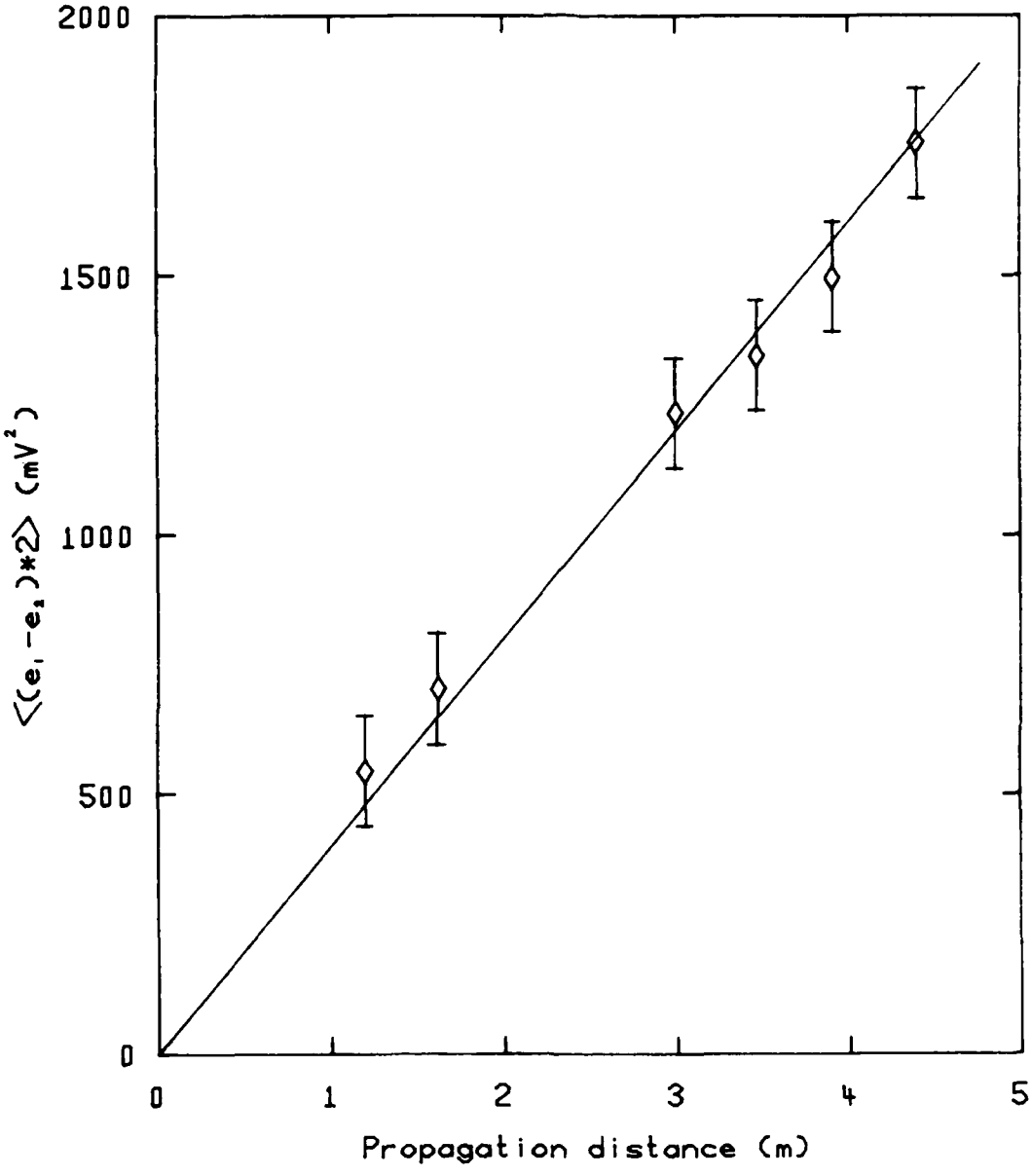

FIGURE 8 - Variance of the difference between the frequency-demodulated heterodyne signals detected simultaneously at two points separated by 15 mm plotted versus the propagation distance for constant turbulence parameters $C_n = 1.05 \times 10^{-4} m^{-1/3}$ and $\ell_o = 2$ mm. The contributions due to the processing noise were subtracted from these data. The error bars represent the standard deviation of the measured noise level for the six data points.

Doppler frequency whereupon tracking is resumed, usually accompanied by a rapid change of the output voltage. On the other hand, if the threshold is set too low, the processor may track a false noise signal and thus give an erroneous output. The problem is most strongly felt in the analysis of the recorded heterodyne signal. Because the dynamic range of the recorder is limited, it is difficult to accommodate the large turbulent amplitude modulations and we find that the signal can fall below the tape noise level. Since the tape noise is in the same frequency range as the frequency $\omega/2\pi$ of the heterodyne signal, the instrument tends to track the noise during these periods. In any case, whether they are due to tracking dropouts or to tracking errors, we observe frequent short peaks in the processor outputs that are correlated with the periods of near-zero amplitude of the recorded heterodyne signal. Through careful adjustments of the recorder dynamic range and of the Doppler Signal Processor threshold, we can minimize these errors but we cannot eliminate them completely. However, since the duration of the peaks are much shorter than the inverse bandwidth of the useful phase signal, they are uncorrelated with the latter. Hence, their contribution to the measured variance of the processor output can be subtracted with good accuracy even though it constitutes a relatively large fraction of the total variance. In the processing of the direct or nonrecorded heterodyne signal, the error peaks can be almost completely eliminated by proper threshold adjustments. Therefore, the residual noise comes mainly from channel No. 2 of Fig. 5b and could be substantially reduced if two Doppler Signal Processors were used to bypass the recording of one of the heterodyne signals.

There are no data points between 2 and 3 m in Fig. 8. This region coincides with the maximum of the scintillation curve, the well-known super-saturation phenomenon. Because of the resulting severe irradiance fluctuations that prevail under these conditions, we were

unable to make the proper recording and processing adjustments that normally minimize and stabilize the noise level. Several measurements were nevertheless made at z = 2.5 m, but the results were unreproducible.

In spite of the difficulties created by the relatively large processing noise, Fig. 8 confirms that the linear relationship given by eq. 17 is consistent. The slope of the regression line can now be used to determine the value of the average velocity $\bar{U}$ of the convection jets or plumes. $\bar{U}$ is the important but yet unspecified parameter of eq. 15. The measured slope is 4.0×10^{-4} V^2/m and from the values of the other parameters, i.e. $K = 10^{-4}$ V/rad/s, $k = 9.93 \times 10^6$ rad/m, $C_n = 1.05 \times 10^{-4}$ $m^{-1/3}$, $\ell_o = 2$ mm, and $\Delta = 15$ mm, it follows from eq. 17 that

$$\bar{U} = 27 \text{ mm/s}. \qquad [18]$$

This value is in excellent agreement with visual observations of the rising convection currents in the turbulence simulator. Therefore, this result constitutes further evidence that eq. 15 is a justified approximation or, more specifically, that the measured time derivative of the turbulent phase is indeed linearly related to the vertical component v_y of the angle of arrival.

3.2 Cross-Correlation of the Angle of Arrival with the Irradiance

The principal objective of this experiment is to verify the assumption of weak correlation between the angle of arrival and the irradiance. Now that the measured $d\phi/dt$ has been proven proportional to the vertical component of the angle of arrival, we can use the simultaneously recorded irradiance and phase-derivative signals to test directly this hypothesis. The results are listed in Table I.

The measurements were performed with the Correlation and Probability Analyzer. The cross-correlation $\langle v_y(I-\langle I\rangle)\rangle$ was estimated by averaging over several measurements of $\langle(v_{y_1}-v_{y_2})(I_1-\langle I_1\rangle)\rangle$ and $\langle(v_{y_1}-v_{y_2})(I_2-\langle I_2\rangle)\rangle$ where the subscripts 1 and 2 refer to the position points r_1 and r_2 in the transverse plane. We find that, within the experimental errors, both expressions give approximately the same value, thus indicating that $|\underset{\sim}{r}_1 - \underset{\sim}{r}_2|$ is sufficiently large for the covariances $\langle v_{y_1}(I_2 - \langle I_2\rangle)\rangle$ and $\langle v_{y_2}(I_1-\langle I_1\rangle)\rangle$ to vanish. Finally, $\langle v_y^2\rangle$ was estimated from the measured $\langle(v_{y_1} - v_{y_2})^2\rangle$ using the theoretical eq. 17 which states that

$$\langle v_y^2\rangle = \frac{1}{2}\left\{1 - (1+8.16\,\Delta^2/\ell_0^2)^{-1/6}\right\}^{-1} \langle(v_{y_1}-v_{y_2})^2\rangle, \qquad [19]$$

where $\Delta = |\underset{\sim}{r}_1 - \underset{\sim}{r}_2| = 15$ mm. The experimental error is relatively large because the cross-correlation value is almost within the instrumental precision.

TABLE I

Comparison of the measured and the predicted cross-correlations between the angle of arrival and the irradiance.
$\gamma = \langle v_y(I - \langle I\rangle)\rangle / \sqrt{\langle v_y^2\rangle\langle (I - \langle I\rangle)^2\rangle}$. z: propagation distance.

z (m)	γ (measured)	γ (predicted, eq. 22)
1.20	0.015 ± 0.04	< 0.023
1.62	0.035 ± 0.04	< 0.034
3.00	0.030 ± 0.04	< 0.074
3.47	0.055 ± 0.04	< 0.087
3.91	0.070 ± 0.04	< 0.100
4.40	0.085 ± 0.04	< 0.112

The results of Table I confirm that the cross-correlation between the angle of arrival $\underset{\sim}{\nu}$ and the irradiance I is indeed small, actually smaller than 8.5% for all data recorded in this experiment. Therefore, the hypothesis of weak correlation between $\underset{\sim}{\nu}$ and I, which is basic to our theoretical model of propagation in turbulence (Refs. 1-3), is validated by direct measurements.

From the theoretical model of Refs. 2-3, we obtain that

$$\frac{\langle v_y(I-\langle I\rangle)\rangle}{\langle v_y^2\rangle^{1/2}\langle(I-\langle I\rangle)^2\rangle^{1/2}} \simeq -\ 0.35\ \frac{C_n^2(k\ell_o)^{1/6}}{n_o}\ z^{4/3}\ \frac{\partial\langle I\rangle/\partial y}{\langle(I-\langle I\rangle)^2\rangle^{1/2}}\ . \quad [20]$$

If $w(z)$ is the radius of a Gaussian beam in turbulence, and if the expression of Ref. 3 for $w(z)$ is used, we have

$$\frac{\langle v_y(I-\langle I\rangle)\rangle}{\langle v_y^2\rangle^{1/2}\langle(I-\langle I\rangle)^2\rangle^{1/2}} \simeq \frac{-0.35(C_n^2/n_o)(k\ell_o)^{1/6}z^{4/3}}{\{w_o^2+0.909(C_n^2/n_o)^2k^{1/6}z^{17/6}\}^{1/2}}\ \frac{\partial\langle I\rangle/\partial(y/w)}{\langle(I-\langle I\rangle)^2\rangle^{1/2}}\ , \quad [21]$$

where w_o is the e-folding radius of the Gaussian source irradiance profile. For the data of Table I, the exact coordinates of the measurement points relative to the beam axis were unfortunately not recorded. Hence, the quantity $|\partial\langle I\rangle/\partial(y/w)|/\langle(I-\langle I\rangle)^2\rangle^{1/2}$ cannot be determined exactly but we can use its maximum value, equal to 0.72 for a Gaussian beam with $\langle(I-\langle I\rangle)^2\rangle^{1/2}/\langle I\rangle = 1.2$, to set a theoretical limit. It thus follows for the conditions of the present experiment that

$$\frac{|\langle v_y(I-\langle I\rangle)\rangle|}{\langle v_y^2\rangle^{1/2}\langle(I-\langle I\rangle)^2\rangle^{1/2}} \lesssim \frac{0.018\ z^{4/3}}{[1\ +\ 0.0024\ z^{17/6}]^{1/2}}\ , \quad [22]$$

where the propagation distance z is expressed in meters.

The numbers derived from eq. 22 are compared with the experimental data in Table I. The ratio of the measurements to the theoretical limits is 65% on the average which constitutes an excellent agreement considering the various approximations made to derive the simple algebraic expression of eq. 22. Therefore, not only is the hypothesis of weak correlation directly verified but its application in Refs. 2-3 to the development of theoretical expressions for the cross-correlation moments is also confirmed by direct comparison with the measurements of $\langle v_y I \rangle$. This conclusion constitutes the principal result and fulfills the main objective of the present study.

3.3 Probability Distribution of the Angle of Arrival

Another important hypothesis made in the development of our propagation model concerns the probability distribution of the angle of arrival $\underset{\sim}{\gamma}$. It was assumed that $\underset{\sim}{\gamma}$ obeys a normal or Gaussian probability-density function which was used to relate the third- and the fourth-order statistical moments of $\underset{\sim}{\gamma}$ to its second-order moments. This hypothesis can now be tested directly from the recorded data of the present experiment.

The probability density functions of the difference between the demodulated heterodyne signals, i.e. $(e(r_1) - e(r_2))$, were calculated at different propagation distances with the Correlation and Probability Analyzer. The instrument provides a 100-point analysis of the density function. For all cases reported here, the electrical voltage $(e(r_1) - e(r_2))$ was sampled at a rate of 500 Hz, and 2^{17} consecutive points were used. A typical measured probability function is plotted in Fig. 9a. Comparison with a least-square fitted Gaussian curve shows that the measured function is not Gaussian as illustrated in Fig. 9a.

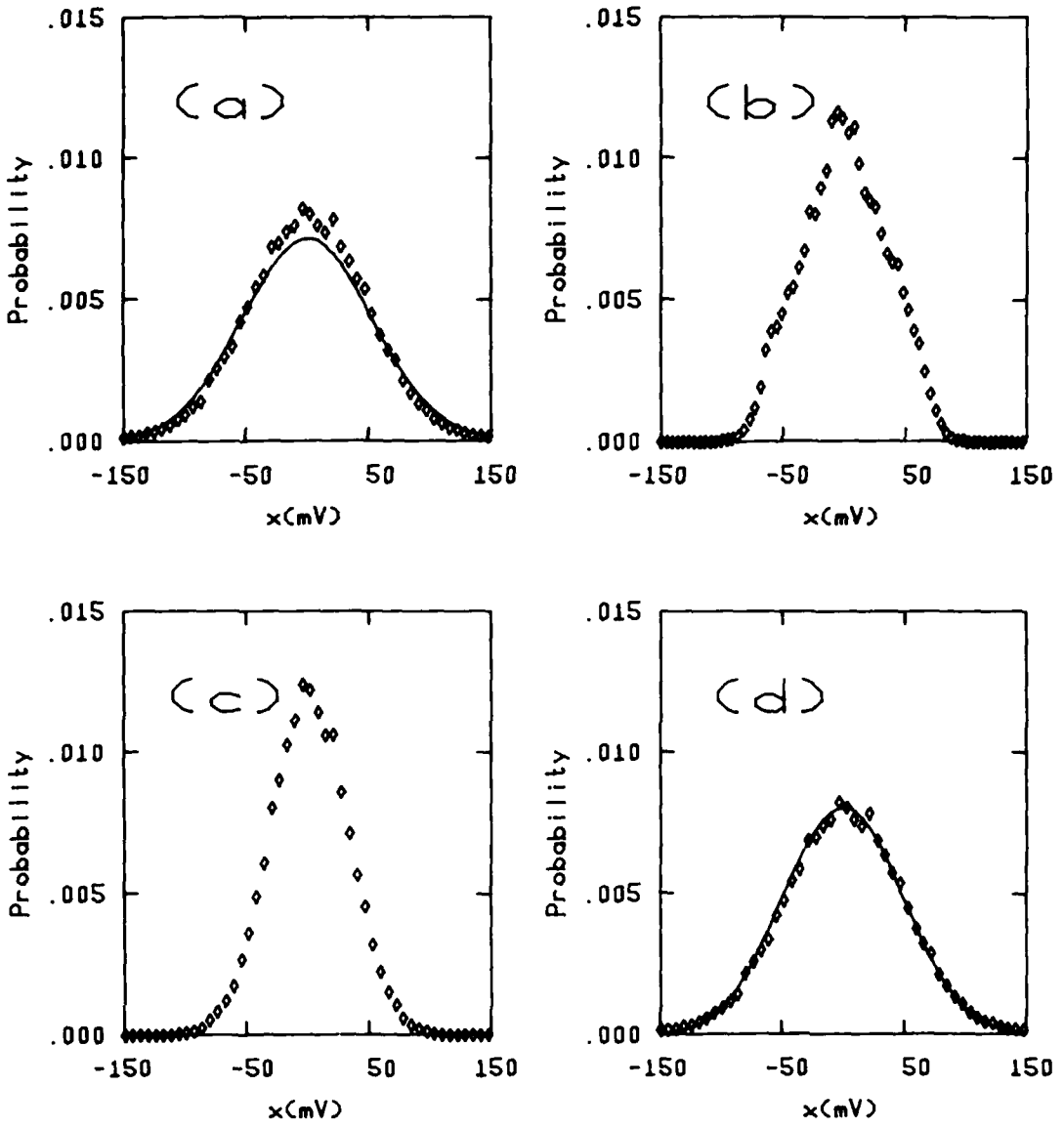

FIGURE 9 - Typical probability density functions used in the analysis of the normal probability assumption for the angle of arrival, z = 3.47 m. (a) measured signal-plus-noise compared with a least-square fitted Gaussian curve (——); (b) measured noise alone; (c) deconvoluted function for the signal alone; (d) comparison of the measured (∇) and reconvoluted (——) functions for the signal-plus-noise.

We have already discussed that the measured random voltage difference $(e(\underset{\sim}{r}_1) - e(\underset{\sim}{r}_2))$ comprises a significant noise contribution. To evaluate the latter, the frequency-demodulated signal from one detector was recorded simultaneously with the heterodyne signal from the same detector. On playing back the tape, the difference $(e(\underset{\sim}{r}_1)-e(\underset{\sim}{r}_2))$ between the recorded demodulated output and the demodulated output of the recorded heterodyne signal, which constitutes a sample of the noise contribution to $(e(\underset{\sim}{r}_1)-e(\underset{\sim}{r}_2))$, can be obtained. For example, the probability density function of the noise sample corresponding to the data of Fig. 9a is drawn in Fig. 9b. It is evident from the observation of these two figures that the standard deviation of the noise is not negligible compared with that of the combined signal-plus-noise. Therefore, a deconvolution is necessary to recover the true probability function of the phase-derivative signal. Indeed, since the noise and the signal are uncorrelated, the measured probability function, $p_e(x)$, is given by the convolution of the respective probability functions of the signal, $p_s(x)$, and of the noise, $p_b(x)$, i.e.

$$p_e(x) = \int_{-\infty}^{\infty} p_s(x-y)\, p_b(y)\, dy \,, \qquad [23]$$

where $p_e(x)$ is defined as the probability that the measured voltage $(e(\underset{\sim}{r}_1) - e(\underset{\sim}{r}_2))$ lies between x and x + dx, and similarly for $p_s(x)$ and $p_b(x)$.

The required function $p_s(x)$ is derived by an iterative method. The approach consists in setting $p_s(x) = A(x) \exp(-\gamma x^2)$ and determining $A(x)$ and γ by successive approximations of the convolution integral of eq. 23. The method was found stable for all cases analyzed in this experiment and it converges after a few iterations. The demodulated

probability function $p_s(x)$ from the experimental data of Figs. 9a-b is plotted in Fig. 9c. By substituting this function $p_s(x)$ back into eq. 23, we can verify the accuracy of the method. This result is illustrated in Fig. 9d where the calculated and the experimental $p_e(x)$ are compared. The agreement is excellent, the root-mean-square difference is less than 2% of the maximum probability, which is of the order of the experimental scatter.

The most straightforward test for Gaussian or normal statistics consists in plotting the experimental probability distributions on a normal probability scale. This is done in Fig. 10 for all the measured deconvoluted probability distributions. If the normal hypothesis is correct, the data must fall on a straight line, which is well verified in Fig. 10 over the range spanning from -4σ to 4σ, where σ is the standard deviation. It is worth emphasizing that the interval $\pm 4\sigma$ encloses the random signal with a probability of 99.98%. Therefore, the hypothesis of normal statistics for $(v_y(\underset{\sim}{r}_1) - v_y(\underset{\sim}{r}_2))$ is fully justified on the basis of this test.

A quantitative measure of the degree of deviation from the hypothetical normal distribution is provided by the well-known chi-square test (Ref. 12). The test is based on the fact that for samples large enough the quantity

$$\chi^2 = \sum_{i=1}^{m} \frac{(f_i - Mp_i)^2}{Mp_i} \qquad [24]$$

has approximately the chi-square distribution with $\nu = m - 1 - s$ degrees of freedom. f_i denotes the number of counts or events registered in the i^{th} channel, p_i is the tested normal probability function, i.e.

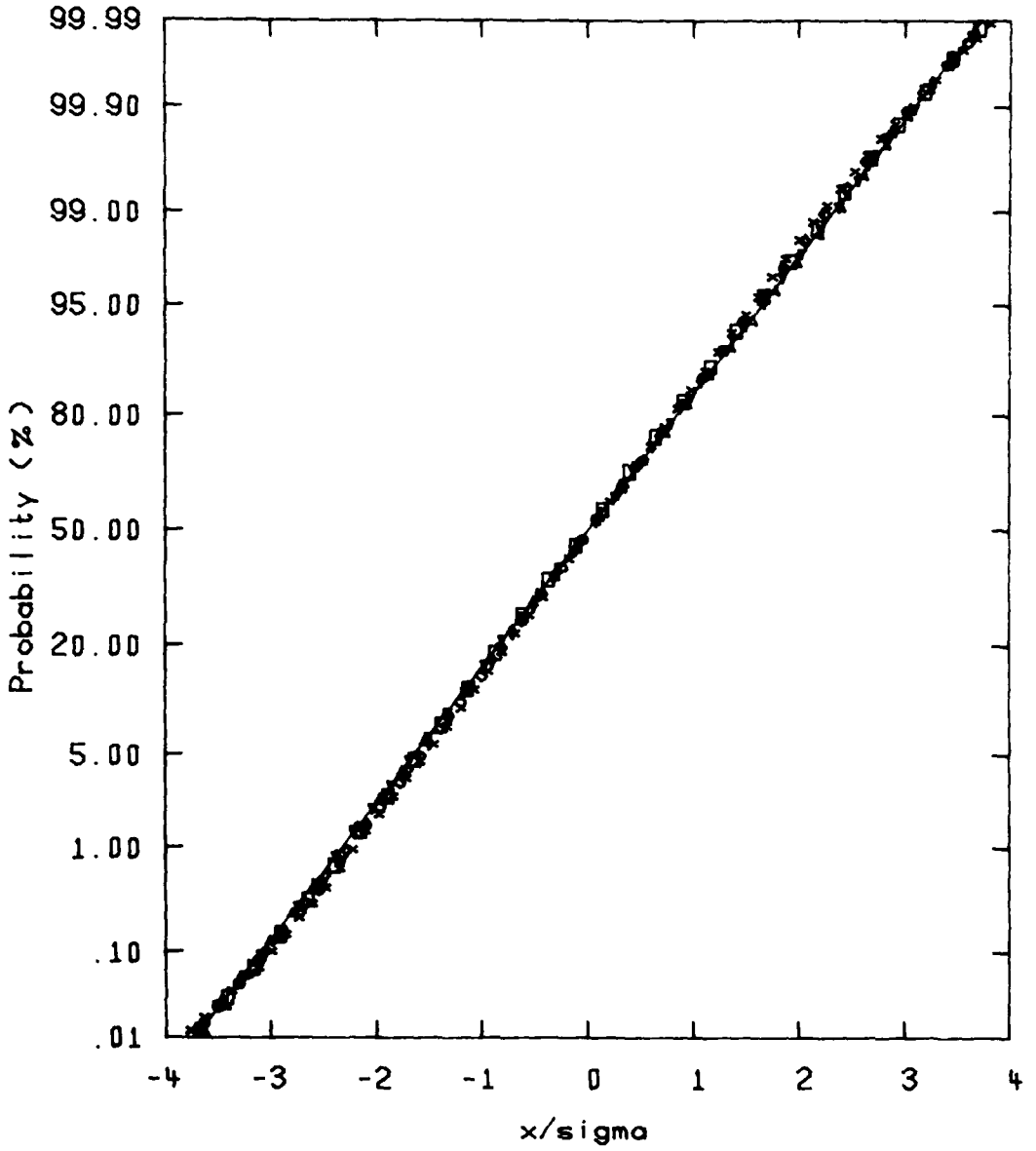

FIGURE 10 - Deconvoluted probability distributions of the difference in the angle of arrival plotted on the normal probability scale versus the centered signal amplitude normalized by the standard deviation σ. The normal distribution is represented by the straight line. ∇: z = 1.20 m; Δ: z = 1.62 m; $\square$: z = 3.00 m; 0: z = 3.47 m; $\diamond$: z = 3.91 m; x: z = 4.40m.

$$p_i = \int_{x_i}^{x_{i+1}} \frac{dx}{\sigma\sqrt{2\pi}} \exp\left[-(x-\mu)^2/2\sigma^2\right] , \qquad [25]$$

M is the size of the sample, and s is the number of parameters estimated from the sample which in this case is equal to 2, the expectation value μ and the standard deviation σ. The test consists in calculating χ^2 according to eq. 24 and comparing the values to the percentiles of the chi-square distribution.

The probability data were calculated from 2^{17} consecutive points sampled at a rate of 500 Hz. Since the correlation time of the signal is typically equal to 30 ms, the number of independent sampled events is about $M \simeq 2^{17}/15 = 8738$. The number of channels provided by the instrument is 100 but regrouping was performed to satisfy the generally accepted condition $f_i \geq 10$ for the test to be significant. The results are listed in Table II. For all cases, we find that $\chi^2 < \chi^2_{97}$ where χ^2_{97} is defined such that

$$P(\chi^2 > \chi^2_{97}) = 97\% \qquad [26]$$

where P is the probability calculated from the chi-square distribution. Therefore, the test shows that the normal probability hypothesis is acceptable on the 97% level, i.e. with a 97% probability of rejecting the hypothesis when in fact it is true, which constitutes a very stringent test.

In summary, the model of normal distribution for the statistics $(v_y(\underset{\sim}{r}_1) - v_y(\underset{\sim}{r}_2))$ is valid with a high degree of accuracy. Since $v_y(\underset{\sim}{r}_1)$ and $v_y(\underset{\sim}{r}_2)$ are nearly independent because of the large relative separation distance $|\underset{\sim}{r}_1 - \underset{\sim}{r}_2| = 15$ mm, and since the convolution of two Gaussian functions gives a Gaussian function, it is highly plausible that the individual $v_y(\underset{\sim}{r}_1)$ and $v_y(\underset{\sim}{r}_2)$ are also normally distributed.

TABLE II

Results of the chi-square test on the normal probability distribution hypothesis for the turbulent angle of arrival. χ^2, chi-square parameter calculed according to eq. 24; χ^2_{97}, 97% - percentile of the chi-square distribution; M, sample size; ℓ, number of degrees of freedom; z, propagation distance.

z (m)	M	ℓ	χ^2	χ^2_{97}
1.20	8738	32	18.0	18.3
1.62	8738	28	11.2	15.6
3.00	8738	22	10.8	11.3
3.47	8738	28	9.2	15.6
3.91	8738	28	11.1	15.6
4.40	8738	42	14.7	26.1

Moreover, because no asymmetry has been observed in the statistical properties of the laser beam, it is equally probable that the horizontal component $v_x(\underset{\sim}{r})$ is also normally distributed. Hence, we conclude that the hypothesis of normal probability distribution of the angle of arrival $\underset{\sim}{\gamma}$, used in the development of our propagation model, is experimentally confirmed with a high degree of confidence.

4.0 DISCUSSION AND CONCLUSION

The application of the heterodyne method to measure the instantaneous turbulent fluctuations of the angle of arrival led to some experimental difficulties. There was the problem of sensitivity to mechanical vibrations which was circumvented by simultaneous detection at two points and subsequent subtraction of the recorded signals. This made it much more difficult to achieve and maintain the proper alignment of the interfering beams. However, the main source of error came from the very nature of the detected phenomenon. Indeed, the heterodyne signals are amplitude modulated by the turbulence over a dynamic range wider than that of the magnetic tape recorder. Consequently, the recorded heterodyne signal frequently falls below the noise level of the recorder which causes random erroneous peaks in the output of the frequency demodulator. Coupled with the relatively small voltage-frequency sensitivity of the instrument used, this produced a low signal-to-noise ratio. Hence, careful attention had to be devoted to all experimental and analytical steps to extract the useful information from the output signal of the frequency demodulator. Meaningful results were nevertheless obtained since the noise and phase contributions are mutually uncorrelated.

Despite the difficulties encountered, our experiment was very successful. It demonstrated that the time derivative of the phase measured from the frequency-demodulated heterodyne signal is indeed linearly related to the vertical component of the angle of arrival. This permitted the calculation of the statistical correlation between the angle of arrival and the irradiance. The hypothesis of weak correlation, which is central to the development of our model of propagation in turbulence (Refs. 1-3), was thus directly confirmed. Also verified were the resulting theoretical predictions for the cross-correlation moments. Finally, the assumption of normal probability distribution for the angle of arrival, which was also used in the construction of our propagation model, is in excellent agreement with the direct probability data of this experiment.

In conclusion, this report confirms, by comparison with measurements, two fundamental assumptions of the DREV propagation model in turbulence. Of course, these had already been proven consistent since the theoretical predictions of Refs. 1-3 regarding the average irradiance and the irradiance variance profiles of laser beams traveling in turbulent media were verified over a wide range of turbulence and beam conditions. The merit of the present experiment consists of the direct verification of these two hypotheses for conditions ranging from the weak to the strong scintillation limits.

5.0 ACKNOWLEDGMENTS

We are pleased to acknowledge the able technical assistance of A. Perreault and R. Rochette in setting up the simulation facility and participating in data acquisition. Preliminary measurements were made by D. Desjardins and M.A. Côté. We would also like to thank Dr. M. Gravel for helpful discussions.

6.0 REFERENCES

1. Bissonnette, L.R., "Average Irradiance and Irradiance Variance of Laser Beams in Turbulent Media", DREV R-4104/78, May 1978, UNCLASSIFIED

2. Bissonnette, L.R. "Modelling of Laser Beam Propagation in Atmospheric Turbulence", pp 73-94, Proceedings of the Second International Symposium on Gas-Flow and Chemical Lasers, John F. Wendt editor, Hemisphere Publishing Corporation, Washington, D.C. (1979).

3. Bissonnette, L.R. "Focused Laser Beams in Turbulent Media", DREV R-4178/80, December 1980. UNCLASSIFIED.

4. Bissonnette, L.R. "Propagation of Adaptively Corrected Laser Beams Through a Turbulent Atmosphere", Journal de Physique, Colloque C9, supplément au no. 11, Tome 41, p. C9-415, 1980.

5. Bissonnette, L.R. "Propagation Model of Adaptively Corrected Laser Beams in Turbulence", DREV R-4200/81, UNCLASSIFIED

6. Durst, F. and Zaré, M., "Removal of pedestals and directional ambiguity of optical anemometer signals", Appl. Opt., Vol. 13, No. 11, p. 2562, 1974.

7. Tatarskii, V.I., "Wave Propagation in a Turbulent Medium", Dover Publication, New York, 1967.

8. DISA Type 55L Laser Doppler Anemometer, Instruction Manual, issued by DISA Information Department, DISA Elecktronik A/S, DK-2740 Skovlunde, Denmark.

9. Bissonnette, L.R. "Laboratory Simulation of Atmospheric Turbulence for Optical Propagation Studies", DREV R-4075/77, August 1977, UNCLASSIFIED

10. Bissonnette, L.R. "Atmospheric Scintillation of Optical and Infrared Waves: a Laboratory Simulation", Appl. Opt., Vol. 16, No. 8, p. 2242, 1977.

11. Vinnichenko, N.K., Pinus, N.Z., Shmeter, S.M., and Shur, G.N., "Turbulence in the Free Atmosphere", translated from Russian, Consultants Bureau, New York - London, 1973.

12. Cramér, Harald, "The Elements of Probability Theory", John Wiley and Sons, New York (1955).

INTERNAL DISTRIBUTION

DREV R-4213/81

1 - Chief
1 - Deputy Chief
1 - Military Assistant
1 - Director Armaments Division
1 - Director Data Systems Division
1 - Director Electro-optics Division
1 - Director Propulsion Division
10 - Document Library
1 - L. Bissonnette (author)
1 - J.F. Boulter
1 - J.C. Anctil
1 - J. Beaulieu
1 - A. Cantin
1 - R. Carbonneau
1 - J.M. Cruickshank
1 - J. Dubois
1 - F. Findlay
1 - M. Gravel
1 - E. Lytle
1 - P. Mathieu
1 - J.P. Morency
1 - G. Morley
1 - G. Otis
1 - P. Pace
1 - J.P. Régnière
1 - P. Roney
1 - W.G. Tam
1 - D. Vincent
1 - K.D. Foster
1 - G. Fournier
1 - T.V. Jacobson
1 - S. Barton
1 - J.M. Garneau

CRDV R-4213/81 (NON CLASSIFIE)

Bureau - Recherche et Développement, MDN, Canada.
CRDV, C.P. 8800, Courcelette, Qué. G0A 1R0

"Statistique des fluctuations de l'angle d'arrivée et de l'intensité lumineuse de faisceaux laser se propageant dans la turbulence"
par L. Bissonnette et R. Côté

La mesure de l'angle d'arrivée en un point à l'intérieur d'un faisceau laser se propageant dans la turbulence est obtenue par la démodulation en fréquence du signal hétérodyne résultant de l'interférence d'un faisceau sonde avec un faisceau de référence. On utilise ensuite ces données pour démontrer que l'angle d'arrivée et l'intensité lumineuse sont faiblement corrélés et que l'angle d'arrivée obéit à une distribution de probabilité normale. Ceci constitue une vérification directe de deux hypothèses fondamentales du modèle de propagation dans la turbulence mis au point au Centre de recherches pour la défense, Valcartier (CRDV). (NC)

CRDV R-4213/81 (NON CLASSIFIE)

Bureau - Recherche et Développement, MDN, Canada.
CRDV, C.P. 8800, Courcelette, Qué. G0A 1R0

"Statistique des fluctuations de l'angle d'arrivée et de l'intensité lumineuse de faisceaux laser se propageant dans la turbulence"
par L. Bissonnette et R. Côté

La mesure de l'angle d'arrivée en un point à l'intérieur d'un faisceau laser se propageant dans la turbulence est obtenue par la démodulation en fréquence du signal hétérodyne résultant de l'interférence d'un faisceau sonde avec un faisceau de référence. On utilise ensuite ces données pour démontrer que l'angle d'arrivée et l'intensité lumineuse sont faiblement corrélés et que l'angle d'arrivée obéit à une distribution de probabilité normale. Ceci constitue une vérification directe de deux hypothèses fondamentales du modèle de propagation dans la turbulence mis au point au Centre de recherches pour la défense, Valcartier (CRDV). (NC)

CRDV R-4213/81 (NON CLASSIFIE)

Bureau - Recherche et Développement, MDN, Canada.
CRDV, C.P. 8800, Courcelette, Qué. G0A 1R0

"Statistique des fluctuations de l'angle d'arrivée et de l'intensité lumineuse de faisceaux laser se propageant dans la turbulence"
par L. Bissonnette et R. Côté

La mesure de l'angle d'arrivée en un point à l'intérieur d'un faisceau laser se propageant dans la turbulence est obtenue par la démodulation en fréquence du signal hétérodyne résultant de l'interférence d'un faisceau sonde avec un faisceau de référence. On utilise ensuite ces données pour démontrer que l'angle d'arrivée et l'intensité lumineuse sont faiblement corrélés et que l'angle d'arrivée obéit à une distribution de probabilité normale. Ceci constitue une vérification directe de deux hypothèses fondamentales du modèle de propagation dans la turbulence mis au point au Centre de recherches pour la défense, Valcartier (CRDV). (NC)

CRDV R-4213/81 (NON CLASSIFIE)

Bureau - Recherche et Développement, MDN, Canada.
CRDV, C.P. 8800, Courcelette, Qué. G0A 1R0

"Statistique des fluctuations de l'angle d'arrivée et de l'intensité lumineuse de faisceaux laser se propageant dans la turbulence"
par L. Bissonnette et R. Côté

La mesure de l'angle d'arrivée en un point à l'intérieur d'un faisceau laser se propageant dans la turbulence est obtenue par la démodulation en fréquence du signal hétérodyne résultant de l'interférence d'un faisceau sonde avec un faisceau de référence. On utilise ensuite ces données pour démontrer que l'angle d'arrivée et l'intensité lumineuse sont faiblement corrélés et que l'angle d'arrivée obéit à une distribution de probabilité normale. Ceci constitue une vérification directe de deux hypothèses fondamentales du modèle de propagation dans la turbulence mis au point au Centre de recherches pour la défense, Valcartier (CRDV). (NC)

DREV R-4213/81 (UNCLASSIFIED)

Research and Development Branch, DND, Canada.
DREV, P.O. Box 8800, Courcelette, Que. G0A 1R0

"Angle of Arrival and Irradiance Statistics of Laser Beams in Turbulence"
by L. Bissonnette and R. Côté

Measurement of the local angle of arrival in a laser beam traveling in turbulence is achieved by frequency demodulating the heterodyne signal derived from the interference of a probe and a reference beam. The resulting data are then used to demonstrate that the statistical correlation between the angle of arrival and the irradiance is weak and that the random angle of arrival is normally distributed. These results constitute a direct confirmation of two fundamental assumptions of the theoretical model of propagation in turbulence previously developed at the Defence Research Establishment Valcartier (DREV). (U)

DREV R-4213/81 (UNCLASSIFIED)

Research and Development Branch, DND, Canada.
DREV, P.O. Box 8800, Courcelette, Que. G0A 1R0

"Angle of Arrival and Irradiance Statistics of Laser Beams in Turbulence"
by L. Bissonnette and R. Côté

Measurement of the local angle of arrival in a laser beam traveling in turbulence is achieved by frequency demodulating the heterodyne signal derived from the interference of a probe and a reference beam. The resulting data are then used to demonstrate that the statistical correlation between the angle of arrival and the irradiance is weak and that the random angle of arrival is normally distributed. These results constitute a direct confirmation of two fundamental assumptions of the theoretical model of propagation in turbulence previously developed at the Defence Research Establishment Valcartier (DREV). (U)

DREV R-4213/81 (UNCLASSIFIED)

Research and Development Branch, DND, Canada.
DREV, P.O. Box 8800, Courcelette, Que. G0A 1R0

"Angle of Arrival and Irradiance Statistics of Laser Beams in Turbulence"
by L. Bissonnette and R. Côté

Measurement of the local angle of arrival in a laser beam traveling in turbulence is achieved by frequency demodulating the heterodyne signal derived from the interference of a probe and a reference beam. The resulting data are then used to demonstrate that the statistical correlation between the angle of arrival and the irradiance is weak and that the random angle of arrival is normally distributed. These results constitute a direct confirmation of two fundamental assumptions of the theoretical model of propagation in turbulence previously developed at the Defence Research Establishment Valcartier (DREV). (U)

DREV R-4213/81 (UNCLASSIFIED)

Research and Development Branch, DND, Canada.
DREV, P.O. Box 8800, Courcelette, Que. G0A 1R0

"Angle of Arrival and Irradiance Statistics of Laser Beams in Turbulence"
by L. Bissonnette and R. Côté

Measurement of the local angle of arrival in a laser beam traveling in turbulence is achieved by frequency demodulating the heterodyne signal derived from the interference of a probe and a reference beam. The resulting data are then used to demonstrate that the statistical correlation between the angle of arrival and the irradiance is weak and that the random angle of arrival is normally distributed. These results constitute a direct confirmation of two fundamental assumptions of the theoretical model of propagation in turbulence previously developed at the Defence Research Establishment Valcartier (DREV). (U)

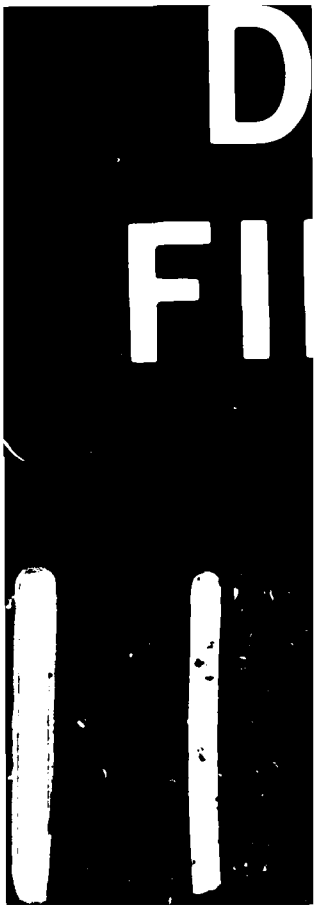
D
FI